JOURNAL OF SOLID STATE CHEMISTRY 115, 174–186 (1995)

Synthesis, Crystal Structures, and Magnetic Properties of Layered Vanadium Oxides: $A_2V_4O_9$ (A = Rb, Cs)

Guo Liu and J. E. Greedan[1]

Institute for Materials Research, McMaster University, 1280 Main Street West, Hamilton, Ontario L8S 4M1, Canada

Received May 10, 1994; in revised form August 1, 1994; accepted August 17, 1994

Single crystals of $Cs_2V_4O_9$ were grown in a CsBr flux and two polytypes of $Cs_2V_4O_9$ have been identified by both single-crystal and powder X-ray diffraction. Phase 1, α-$Cs_2V_4O_9$, crystallizes in the tetragonal system, space group $P4_2/m$, with $a = 5.727(1)$ Å, $c = 15.052(3)$ Å, $Z = 2$, and its structure has been refined based on F^2 to $R1 = 0.0809$, $wR2 = 0.1015$ using all 1450 independent reflections from a nearly perfectly twinned crystal. Phase 2, β-$Cs_2V_4O_9$, also crystallizes in the tetragonal system, space group $I\bar{4}2d$, with $a = 5.726(2)$ Å, $c = 30.062(8)$ Å, $Z = 4$, and its structure has been refined to $R1 = 0.0475$, $wR2 = 0.0805$ using all 537 independent reflections. Both structures consist of VO_5 square pyramids that are linked by edge- and corner-sharing to form two-dimensional arrays with the alkali metals lying between the layers. $Rb_2V_4O_9$ is isostructural with α-$Cs_2V_4O_9$, and its structure has been refined using powder neutron and X-ray diffraction data. Rietveld analysis using powder X-ray diffraction data has confirmed that the α and β phases coexist in the polycrystals of $Cs_2V_4O_9$ with a ratio of $\alpha:\beta \approx 55:45$. Magnetic properties were examined in the temperature range from 5 to 700 K. $Rb_2V_4O_9$ and $Cs_2V_4O_9$ exhibit antiferromagnetic short-range correlations at high temperatures. Consistent with the crystal structures, the magnetic behavior can be explained based on a two-dimensional Heisenberg model and the inductive mechanism proposed previously for similar vanadium oxides.

INTRODUCTION

V(IV)-rich mixed oxides with the alkaline earth and other divalent cations tend to form two-dimensional structures consisting of VO_5 square pyramids. The structures and magnetic properties of the AV_3O_7 series (A = Cd, Ca, Sr) have been the subjects of recent investigations (1, 2). It was found that the magnetic coupling constant $|J|$ increases with increasing ionic radius of the divalent cation A. This was explained on the basis of an inductive mechanism (2). That is, the magnetic exchange was correlated to the basicity of A which increases with increasing ionic radius.

According to the inductive mechanism, similar vanadium oxides of more basic cations than Sr^{2+} will probably show enhanced magnetic exchange interactions. The heavy alkali ions are logical choices for such investigations. Apparently the inductive mechanism does not apply to the fresnoite-type vanadium oxides, $A_2V_3O_8$ (A = K, Rb, NH_4), which contain both V(IV) and V(V) (as diamagnetic VO_4^{3-}) oxidation states where magnetic VO_5^{6-} square pyramids are isolated (3). Thus oxides containing only V(IV) are more likely candidates for this purpose.

It has long been known that there exist a few stoichiometric oxides of V(IV) with the heavy alkalis. Two such interesting compounds, $Rb_2V_4O_9$ (4) and $Cs_2V_4O_9$ (5), have been reported. Prior to this work very little was known about these phases; even their powder patterns were not indexed. In order to further understand the inductive mechanism, we investigated these two compounds. Results on the novel crystal structures and interesting magnetic properties are presented here.

EXPERIMENTAL

Materials Preparation

V_2O_3 was prepared by reducing V_2O_5 (99.9%, Cerac) in H_2 at 900°C. $RbVO_3$ and $CsVO_3$ were prepared by heating in platinum crucibles stoichiometric mixtures of Rb_2CO_3 or Cs_2CO_3 (Johnson Matthey Catalog Company, 99.8% for Rb_2CO_3 and 99.9% for Cs_2CO_3 on metal basis) and V_2O_5 at 600°C for 12–24 hr. Handling involving the carbonates and the reaction products was performed in an argon-filled glove box.

$Rb_2V_4O_9$. A 2:1 mixture of $RbVO_3$ and V_2O_3 was ground intimately in the glove box, pelleted in air and sealed in pyrex under vacuum, heated to 500°C overnight, and finally heated to 550°C for 5–10 hr. The pellets were insulating and black on the surface. Pulverized specimens were dark brown. $Cs_2V_4O_9$ was prepared in the same way but at a slightly lower temperature, 510°C, for overnight. The product was also brown and insulating.

[1] To whom correspondence should be addressed.

0022-4596/95 $6.00

Crystal Growth

A mixture of about 10% $Cs_2V_4O_9$ and 90% predried CsBr (99.9%, Cerac) was sealed in quartz, evacuated to 4×10^{-4} Torr, heated slightly to remove absorbed moisture and sealed off. It was heated slowly to 700°C, soaked for 20 min, then cooled at 6°C/hr to 470°C, and finally cooled rapidly to room temperature. The CsBr flux was removed by washing with distilled water. Plate-like black crystals were obtained. The quartz tube was attacked slightly. Attempts to grow $Rb_2V_4O_9$ crystals at 750°C using a RbBr flux have not been successful.

Powder X-Ray and Neutron Diffraction

Polycrystalline specimens were examined using a 100-mm-diameter Guinier–Hägg camera with Cu $K\alpha_1$ radiation and a silicon internal standard. Procedures for powder X-ray diffraction, including data collection (6), and for ambient and low-temperature neutron diffraction (7) have been described previously. Data processing was effected on an IBM-compatible 80486 personal computer. The program TREOR90P, a PC version of the TREOR program (8) was used for powder pattern indexing. Rietveld refinement was effected using the program DBWS-9006PC by Sakthivel and Young, which is a 1992 release of the PC version of the DBWS3.2S program by Wiles and Young (9).

Single-Crystal X-Ray Diffraction

Crystals suitable for structure analysis were mounted on tips of glass fibers using epoxy cement. Data were collected on a Siemens P3 four-circle diffractometer with Ag $K\alpha$ radiation. Data reduction and structure solution were also performed on an 80486 PC using the Siemens SHELXTL PC (release 4.2, 1991) software package. Azimuthally scanned data were used for absorption corrections and scattering factors of neutral atoms have been employed. Crystal structures were refined using the program SHELXL, part of the SHELXL-92 gamma test version released in 1993. SHELXL refines crystal structures against F^2 instead of the conventional F data, and has the capability of handling twinned crystals that is based on the method of Pratt *et al.* (10). As a result the $wR2$-factor is usually much higher than the conventional R ($R1$ in SHELXL).

Magnetic Measurement and Thermal Analysis

Magnetic moments for polycrystalline samples were obtained using Quantum design SQUID magnetometers. Data in the temperature range from 5 to 300 K were obtained at McMaster University. Data from 300 to 700 K (710 K for $Cs_2V_4O_9$) were taken in the Novel Materials Laboratory at the University of California at Davis. Samples used for the high-temperature measurement were sealed in quartz under vacuum. The two data sets were merged on the scale of the low-temperature data where larger amounts of samples were used and the data were believed to be more accurate. Diamagnetic corrections have been applied according to Selwood (11).

Thermogravimetric analysis (TGA) was performed for $Cs_2V_4O_9$ and $Rb_2V_4O_9$ with a Netzsch STA 409 thermal analyzer in flowing O_2 atmosphere at a 5°C/min heating rate to 600°C. Differential scanning calorimetry (DSC) data were obtained in N_2 with a 2910 DSC analyzer by TA Instruments at 5°C/min to 400°C.

RESULTS AND DISCUSSION

Single-Crystal X-Ray Diffraction of $Cs_2V_4O_9$

α-$Cs_2V_4O_9$. The first crystal examined was found to belong to the primitive tetragonal system with a = 5.731(2) Å and c = 15.065(7) Å. Systematic extinction conditions were consistent with the space groups $P4_2/m$ (No. 84), $P4_2$ (No. 77), and $P4_222$ (No. 93). Intensity statistics suggested the most likely space group to be the centrosymmetric $P4_2/m$. Positional parameters of the heavy atoms (Cs and V) were located by direct methods and oxygens by difference Fourier. Full matrix least-squares refinement of the structure using reflections with $F_o^2 > 2\sigma(F_o^2)$ and anisotropic thermal parameters gave a large conventional R-factor, 0.12. It was found that profiles of some intense reflections were highly asymmetric, suggesting that the crystal was probably not single. Hence a second crystal was examined. Incidently, it turned out to be a second polytype as will be described below. Thus a third crystal was investigated.

The third plate-like crystal was examined by a precession camera using Mo $K\alpha$ radiation to verify its symmetry and quality prior to data collection on the diffractometer. Its unit cell parameters, a = 5.727(1) Å and c = 15.052(3) Å, which were determined by the diffractometer from 25 low angle reflections, were slightly smaller than those of the first crystal. The most probable space group and the best structure solution were found to be the same as with the first crystal. However, the convergence was even worse, $R \approx 0.23$ with reflections of $F_o^2 > 2\sigma(F_o^2)$. There existed numerous electron residues in the difference Fourier which gave the appearance of a high level of disorder, but the refinement did not improve significantly even if disordering was considered. Instead, the atomic parameters were unstable with unusually large estimated standard deviations.

Given the fact that the precession photographs did not reveal any obvious twinning, this "disorder" behavior was suspected to be caused by twinning by merohedry which is known to be undetectable by photographic

methods, but correct space groups are obtainable and structure solutions can be achieved (12). This assumption was tested using the program SHELXL. Upon introduction of a TWIN matrix (Table 1) corresponding to one twin component being related to the other by the interchange of the *a*- and *b*-axes, the refinement converged immediately. The final parameters and crystallographic data are compiled in Table 1. All structural parameters are reasonable.

It is interesting to note that when the same TWIN matrix was used for the first data set, no improvement was achieved, while the twin components for the third crystal were nearly of equal sizes. The batch scale factor, BASF, namely, the fraction of one twin component in this case, was refined to 0.505(3). This result suggests that the crystal was almost perfectly twinned. This is somewhat unusual and raises questions about the space group. The noncentrosymmetric space group $P4_2$ was thus tested.

TABLE 1[a]

Crystal Data and Data Collection and Structure Refinement Details for α- and β-$Cs_2V_4O_9$

Diffractometer	Siemens P3	
Radiation	Ag$K\alpha$ (λ = 0.56086 Å)	
Temperature (K)	293(2)	
Monochromator	Highly oriented graphite crystal	
Scan type	ω	
Scan speed	Variable; 2.00 to 29.30°/min. in ω	
Scan range (ω)	0.06°	
Background	Stationary crystal and stationary counter at beginning and end of scan, each for 0.5% of total scan time	
Standard reflections	3 measured every 100 reflections	
System used	Siemens SHELXTL PLUS (PC Version), SHELXL-92	
Refinement method	Full-matrix least-squares on F^2	
Quantity minimized	$wR2$ as defined below	
Formula	α-$Cs_2V_4O_9$	β-$Cs_2V_4O_9$
Crystal system	Tetragonal	Tetragonal
Space group	$P4_2/m$	$I\bar{4}2d$
Unit cell dimensions (Å)	a = 5.727(1)	a = 5.726(2)
	c= 15.052(3)	c = 30.062(8)
Volume (Å^3)	493.7(2)	985.6(6)
Z	2	4
Density (calc. g/cm^3)	4.128	4.135
Absorption coefficient (mm^{-1})	5.730	5.740
F(000)	548	1096
Crystal size (mm^3)	0.11 × 0.11 × 0.054	0.19 × 0.18 × 0.09
2θ range (°)	5.62 to 60.12	4.28 to 50.12
Index ranges	$-10 \le h \le 10$	$0 \le h \le 8$
	$0 \le k \le 10$	$0 \le k \le 8$
	$0 \le l \le 26$	$0 \le l \le 45$
Reflections collected	2554	1012
Independent reflections	1450 [R(int) = 0.0464]	537 [R(int) = 0.0882]
Data/restraints/parameters	1450/0/37	537/0/35
Goodness-of-fit on F^2	0.912	0.969
R indices [$I > 2\sigma(I)$]	$R1$ = 0.0473, $wR2$ = 0.0908	$R1$ = 0.0386, $wR2$ = 0.0779
R indices (all data)	$R1$ = 0.0809, $wR2$ = 0.1015	$R1$ = 0.0475, $wR2$ = 0.0805
TWIN matrix	0 1 0 1 0 0 0 0 −1	—
Twin component BASF	0.505(3)	—
Flack absolute structure factor	—	0.1(2)
Largest diff. peak and hole (e/Å^3)	1.7 and −2.9	1.7 and −1.4

Note. $R1 = (\Sigma||F_o| - |F_c||)/\Sigma|F_o|$; $wR2 = [\Sigma w(F_o^2 - F_c^2)^2/\Sigma w(F_o^2)^2]^{1/2}$; GooF = $s = [\Sigma w(F_o^2 - F_c^2)^2/(n - p)]^{1/2}$.

[a] See NAPS document No. 05155 for 6 pages of supplementary materials. This is not a multi-article document. Order from NAPS c/o Microfiche Publications, P. O. Box 3513 Grand Center Station, NY 10163-3513. Remit in advance, in U.S. funds only, $7.75 for photocopies or $4.00 for microfiche. There is a $15.00 invoicing charge on all orders filled before payment. Outside U.S. and some parts of Canada add postage of $4.50 for the first 20 pages and $1.00 for each 10 pages of material thereafter, or $1.75 for the first microfiche and $0.50 for each fiche thereafter.

Refinement converged roughly to the same level. However, strong correlations among some atom pairs, nonpositive definite thermal parameters, and large estimated standard deviations clearly indicate rejection of the noncentrosymmetric space group. Not surprisingly, this structure could not be properly described in other space groups belonging to the 4 or $\bar{4}$ point groups. $P4_2/m$ is believed to be the correct space group. As will be shown later, powder X-ray diffraction data tend to support this space group as well.

β-$Cs_2V_4O_9$. The second crystal was found to have a body-centered tetragonal symmetry. The unit cell parameters derived from 18 reflections with $2\theta < 30°$, a = 5.726(2) Å and c = 30.062(8) Å, appeared to be closely related to those of α-$Cs_2V_4O_9$. In order to check for the possibility of the existence of a supercell or an accidental doubling of the c-axis of the same unit cell already described above, data were actually collected based a primitive cell. The results were convincing that this crystal was indeed a new phase with the body-centered symmetry.

Systematic extinction conditions were consistent with the noncentrosymmetric space groups $I\bar{4}2d$ (No. 122) and $I4_1md$ (No. 109). Intensity statistics and combined figures of merits suggested the most likely space group to be $I\bar{4}2d$. Essentially all atoms were located by direct methods. The positional and anisotropic thermal parameters were refined by full matrix least-squares methods to $R1$ = 0.0475 using all 537 independent reflections. On the other hand, no reasonable structure solution could be obtained in the space group $I4_1md$ by direct or Patterson methods, nor could the given structure be refined properly in $I4_1md$. The successful refinement and the chemically meaningful results of the structure in $I\bar{4}2d$ are good indications for a correct space group. The Flack absolute structure parameter (13, 14), x = 0.1(2), is within 1σ of zero, suggesting that the structure is assigned correctly for this noncentrosymmetric space group. Crystallographic data are also compiled in Table 1.

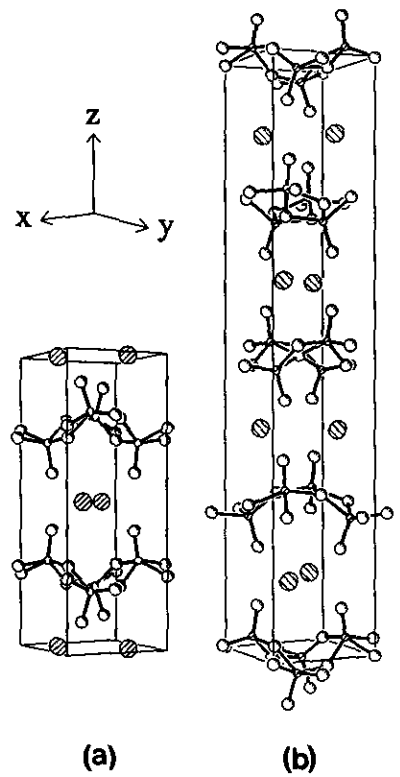

FIG. 1. Crystal structure of (a) α-$Cs_2V_4O_9$ and (b) β-$Cs_2V_4O_9$. Only the VO_5 square pyramids are outlined. Large shaded circles represent Cs^+ ions.

TABLE 2

Atomic Coordinates and Equivalent Isotropic and Anisotropic Displacement Parameters (Å² × 10³) for α- and β-$Cs_2V_4O_9$

Atom	Site	x	y	z	U_{11}	U_{22}	U_{33}	U_{23}	U_{13}	U_{12}	U(eq)
					α-$Cs_2V_4O_9$						
Cs	4*j*	0.2763(1)	0.2513(1)	0.5	20(1)	19(1)	28(1)	0	0	−1(1)	22(1)
V	8*k*	0.2947(1)	0.1365(2)	0.2018(1)	8(1)	9(1)	13(1)	0(1)	−1(1)	−1(1)	10(1)
O(1)	2*a*	0	0	0.25	10(2)	U_{11}	20(3)	0	0	0	13(1)
O(2)	8*k*	0.2371(7)	0.2071(7)	0.0996(3)	19(2)	26(2)	15(2)	4(1)	−3(1)	−4(2)	20(1)
O(3)	8*k*	0.1905(6)	0.3774(6)	0.2834(2)	10(1)	10(1)	22(2)	−2(1)	1(1)	−1(1)	14(1)
					β-$Cs_2V_4O_9$						
Cs	8*d*	0.2747(2)	0.25	0.125	23(1)	21(1)	25(1)	−1(1)	0	0	23(1)
V	16*e*	0.2943(3)	0.1366(2)	−0.0241(1)	12(1)	13(1)	11(1)	1(1)	1(1)	0(1)	12(1)
O(1)	4*a*	0	0	0	5(3)	U_{11}	19(5)	0	0	0	10(2)
O(2)	16*e*	0.2396(13)	0.2064(11)	−0.0752(2)	28(3)	15(3)	16(2)	3(2)	1(2)	6(3)	20(1)
O(3)	16*e*	0.1933(11)	0.3761(12)	0.0165(2)	13(3)	17(3)	19(2)	−4(2)	1(2)	−3(3)	17(1)

Note. U(eq) is defined as one-third of the trace of the orthogonalized U_{ij} tensor. The anisotropic displacement factor exponent takes the form $-2\pi^2 [h^2 a^{*2} U_{11} + \cdots + 2 h k a^* b^* U_{12}]$.

TABLE 3
Selected Bond Lengths (Å), Bond Angles (°), and Bond Valence Sums (BVS) for $Cs_2V_4O_9$ and $Rb_2V_4O_9$

α-$Cs_2V_4O_9$			β-$Cs_2V_4O_9$			$Rb_2V_4O_9$		
Cs–O(2)	×2	3.149(4)	Cs–O(2)	×2	3.135(6)	Rb–O(2)	×2	3.072(17)
Cs–O(2)′	×2	3.198(4)	Cs–O(2)′	×2	3.202(7)	Rb–O(2)′	×2	3.203(19)
Cs–O(2)″	×2	3.315(4)	Cs–O(2)″	×2	3.307(7)	Rb–O(2)″	×2	3.282(18)
Cs–O(2)‴	×2	3.318(4)	Cs–O(2)‴	×2	3.328(6)	Rb–O(2)‴	×2	3.148(19)
Cs–O(3)	×2	3.376(4)	Cs–O(3)	×2	3.374(5)	Rb–O(3)	×2	3.107(16)
Mean		3.271(4)	Mean		3.269(6)	Mean		3.162(18)
BVS(Cs) = 1.02			BVS(Cs) = 1.03			BVS(Cs) = 0.90		
V–O(2)		1.624(4)	V–O(2)		1.619(5)	V–O(2)		1.616(12)
V–O(3)		1.916(4)	V–O(3)		1.923(6)	V–O(3)		2.058(16)
V–O(3)′		1.941(4)	V–O(3)′		1.929(7)	V–O(3)		2.150(18)
V–O(3)″		1.945(4)	V–O(3)″		1.960(6)	V–O(3)″		1.667(16)
V–O(1)		1.9964(8)	V–O(1)		1.994(2)	V–O(1)		2.149(10)
Mean		1.884(4)	Mean		1.885(5)	Mean		1.928(14)
BVS (V) = 4.11			BVS(V) = 4.11			BVS(V) = 4.17		
V–V′		2.824(2)	V–V′		2.828(3)	V–V′		2.735(20)
V–V″		3.004(1)	V–V″		3.000(2)	V–V″		3.213(13)
O(1)–O(3)		2.473(5)	O(1)–O(3)		2.471(5)	O(2)–O(3)		2.506(30)
O(2)–V–O(3)		105.6(2)	O(2)–V–O(3)		111.6(3)	O(2)–V–O(3)		116.5(9)
O(2)–V–O(3)′		111.1(2)	O(2)–V–O(3)′		105.1(3)	O(2)–V–O(3)′		107.1(8)
O(3)–V–O(3)′		96.5(2)	O(3)–V–O(3)′		95.7(3)	O(2)–V–O(3)″		99.5(9)
O(2)–V–O(3)″		113.4(2)	O(2)–V–O(3)″		113.3(3)	O(2)–V–O(1)		104.8(8)
O(3)–V–O(3)″		84.4(2)	O(3)–V–O(3)″		133.2(2)	O(3)–V–O(3)′		133.2(7)
O(3)′–V–O(3)″		133.4(1)	O(3)′–V–O(3)″		85.1(3)	O(3)–V–O(3)″		99.2(8)
O(2)–V–O(1)		105.7(1)	O(2)–V–O(1)		106.1(3)	O(3)–V–O(1)		77.5(5)
O(3)–V–O(1)		148.1(2)	O(3)–V–O(1)		78.2(2)	O(3)′–V–O(3)″		89.4(7)
O(3)′–V–O(1)		77.8(1)	O(3)′–V–O(1)		148.2(2)	O(3)′–V–O(1)		75.6(5)
O(3)″–V–O(1)		77.7(1)	O(3)″–V–O(1)		77.4(2)	O(3)″–V–O(1)		154.2(7)

Cystal Structures

α-$Cs_2V_4O_9$. Atomic parameters including anisotropic thermal parameters are listed in Table 2. Important bond lengths, bond angles, and bond valence sums (BVS) (15) are listed in Table 3. The BVS values for Cs and V are consistent with their formal oxidation states. The crystal structure is shown in Fig. 1a. It can be described as a two-layer structure that consists of VO_5 square pyramids linked by edge- and corner-sharing to form V–O layers. The large Cs^+ ions occupy holes between the layers. The molecular geometry of a VO_5 coordination polyhedron is shown in Fig. 2a. It is similar to other VO_5 square pyramids found in layered V(IV) oxides such as AV_3O_7 (A = Ca, Cd, Sr) (1, 2) and CaV_4O_9 (16) where a short, double-bond-like (axial) V–O with a bond length ranging from 1.58 to 1.62 Å was also present. In α-$Cs_2V_4O_9$, a square-planar-like eight-member ring with four oxygens and four vanadium atoms is formed when four neighboring VO_5 are linked by corner-sharing in such a way that the axial V–O bonds of two opposite VO_5 point upward while the other two point downward (Fig. 3a). A Cs^+ ion is then located roughly above one ring oxygen and bonded to four nearest axial oxygens from VO_5 pointing to the same side of a V–O layer. Due to the location of Cs^+ ions on mirror planes perpendicular to the c-axis, the coordination of Cs^+ is the same from the V–O layer above and below it. Thus the Cs^+ is 10-coordinated and the CsO_{10} geometry can be roughly described as a bicapped

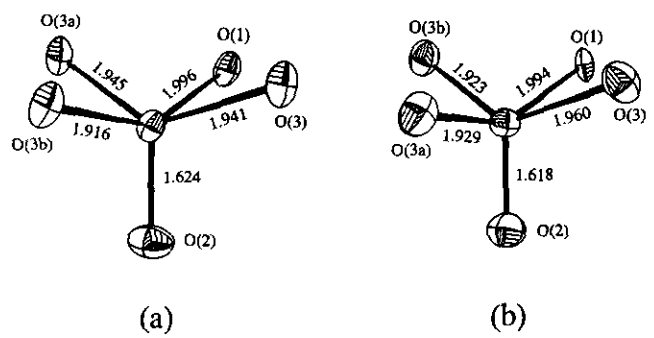

FIG. 2. Molecular geometry of a VO_5 square pyramid in (a) α-$Cs_2V_4O_9$ and (b) β-$Cs_2V_4O_9$. Atoms are plotted at 90% probability level.

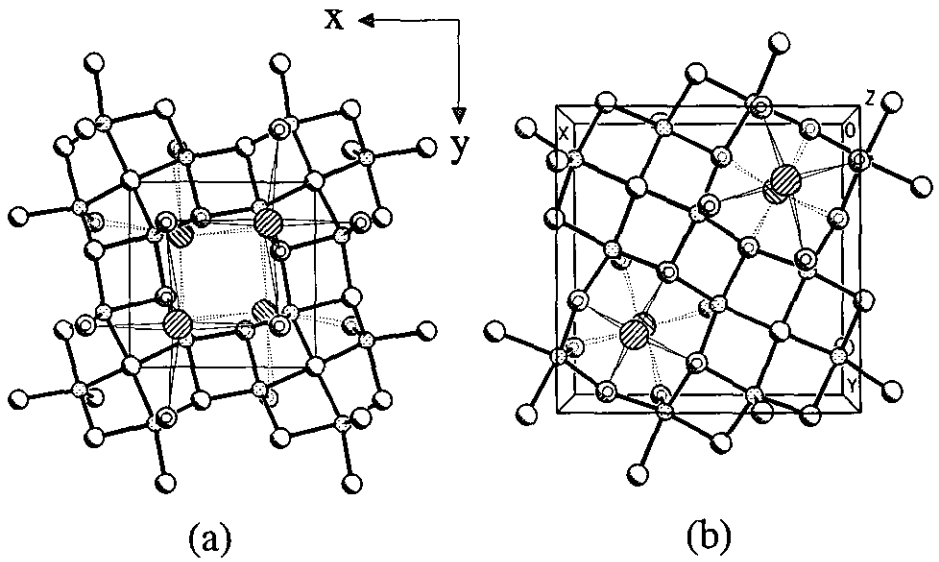

FIG. 3. A typical V–O layer in (a) α- and β-$Cs_2V_4O_9$ and (b) CaV_4O_9. Small circles represent V atoms, intermediate ones for O, and large shaded ones for Cs^+ or Ca^{2+} ions. Double circles highlight those oxygens bonded to Cs^+ or Ca^{2+}.

(Cs–O(3)) square prism. The CsO_{10} polyhedron is viewed from two different orientations in Figs. 4a and 4b, where the existence of a mirror plane is clear.

It is interesting tc compare the α-$Cs_2V_4O_9$ structure with the single-layer CaV_4O_9 (16) (tetragonal, $P4/n$, a = 8.333(5) Å and c = 5.008(3) Å) and the two-layer structure of the AV_3O_7 (A = Cd, Ca, Sr; orthorhombic) system. One V–O layer of CaV_4O_9 is shown in Fig. 3b. The V–O layers in AV_3O_7 are very similar (2, 17) to Fig. 3b. In the latter two structures, eight-membered rings similar to the one just described also exist but are formed by four VO_5 axial oxygen atoms pointing to the same side of a V–O layer. A Ca^{2+} or A^{2+} ion is bonded with four axial oxygens from the layer below it and four ring oxygens from the layer above it. The CaO_8 and AO_8 geometries are thus square antiprismatic. Unlike the Cs^+ ions in α-$Cs_2V_4O_9$ the Ca^{2+} or A^{2+} ions are located in the center of channels parallel to the c-axis, which are formed by the eight-membered rings. The size of the O_8 hole is apparently too small to fit the much larger Cs^+ ion. Therefore, the VO_5 polyhedra in α-$Cs_2V_4O_9$ have to adopt a different linkage.

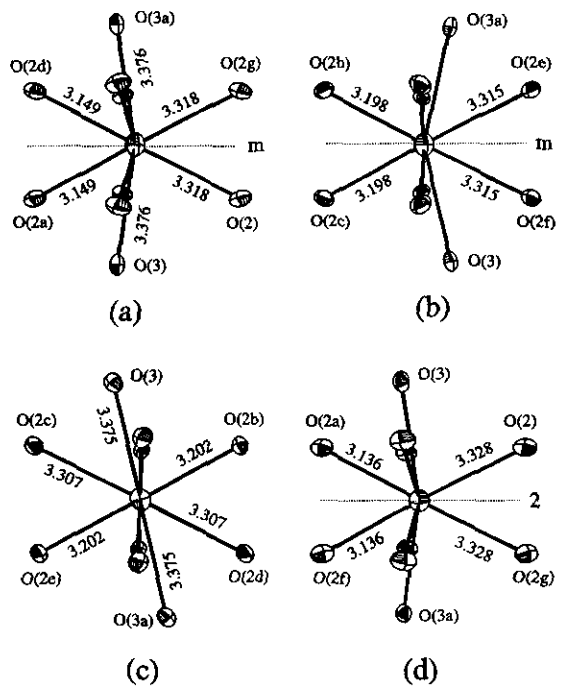

FIG. 4. Molecular geometry of a CsO_{10} polyhedron in (a) and (b) α-$Cs_2V_4O_9$ and (c) and (d) β-$Cs_2V_4O_9$. (a) and (c) are a-axis projections; (b) and (d) are b-axis projections. Atoms are plotted at 90% probability level.

The titanium analogue of $Cs_2V_4O_9$, namely, $Cs_2Ti_4O_9$, has a totally different structure even though Ti(IV) and V(IV) have very similar ionic radii (18). Its powder X-ray diffraction pattern suggested that $Cs_2Ti_4O_9$ (19) was probably isostructural with the monoclinic $Tl_2Ti_4O_9$ (20) which has a sheet structure based on an octahedral TiO_6 coordination. These results reflect the fundamental difference in chemical bonding between Ti(IV) and V(IV). The later has a strong tendency to form vanadyl oxides which are characterized by the short, double V=O bond as described above.

$Cs_2V_4O_9$ may be considered to be a special case of the vanadium oxide bronzes (VOBs). The structural chemistry of some VOBs has been reviewed recently (21). Only a few VOBs of the heavy alkalis (Rb, Cs) have been well

characterized. In general, V(IV) adapts the same square pyramidal coordination in all these compounds. The existence of V(V) in VOBs could add another coordination mode, the VO_4 tetrahedron. In the relatively alkali-rich VOBs such as CsV_2O_5 (22), $Cs_2V_5O_{13}$ (23), and $Rb_2V_3O_8$ (3, 24) there clearly exist discrete VO_5^{6-} and VO_4^{3-} coordination polyhedra. This case is in fact very similar to many vanadyl phosphates such as $A_2VOP_2O_7$ (A = K, Rb, Cs) (25) and $AVOPO_4$ (A = Rb, Cs) (26) where a tetrahedral PO_4 coordination is the rule. The alkali-poor VOBs such as $Cs_{0.3}V_2O_5$ (27) and $Cs_{0.35}V_3O_7$ (28), on the other hand, contain VO_5 square pyramids only, and are thus similar to V_2O_5 (21) and α-$Cs_2V_4O_9$, but the square pyramids are linked to form hexagonal tunnel structures. Therefore, the α-$Cs_2V_4O_9$ structure is unique among these vanadium compounds with the heavy alkalis because it consists of VO_5 square pyramids only and has a distinct layered structure. As a result the Cs^+ coordination in α-$Cs_2V_4O_9$ is also different from those in the VOB's and vanadyl phosphates just mentioned.

β-$Cs_2V_4O_9$. Atomic parameters are also listed in Table 2. Selected bond lengths, bond angles and BVS values are compiled in Table 3. Again the BVS values for Cs and V are consistent with their formal oxidation states. The structure is shown in Fig. 1b. It can be described as a four-layer structure that consists of V–O layers very similar to those found in α-$Cs_2V_4O_9$.

The c-axis of β-$Cs_2V_4O_9$ is almost exactly twice that of α-$Cs_2V_4O_9$, and the a-axes are essentially identical for both lattices. These results suggest that the two structures may be closely related. In fact, the average V–O bond length for β-$Cs_2V_4O_9$ is nearly identical with that for α-$Cs_2V_4O_9$, the VO_5 molecular geometries are remarkably similar (Fig. 2 and Table 3), and the linkage of VO_5 in a V–O layer is virtually the same as in Fig. 3a. The major difference lies in the stacking sequence of these layers. This can be better seen by looking at the V positions in both structures as shown in Fig. 5. It is worth noting that the VO_5 square pyramids are tilted with respect to the c-axis, and the V atoms in a V–O layer are not exactly in the same plane. In Fig. 5a, V atoms in the two layers of the α-type structure are viewed down the c-axis; they are related by a mirror plane perpendicular to the c-axis and thus can be roughly described as having an eclipsed configuration. In Fig. 5b, only two layers of V atoms of the β-type structure are shown for clarity. Each layer is basically the same as that in the α form. However, the two layers are clearly shifted and rotated. As a result of this difference, the Cs^+ coordination in β-$Cs_2V_4O_9$ is slightly different from that in the α form. This is demonstrated in Fig. 4. The projections in Figs. 4c and 4d show that the mirror plane in the α form is now replaced by a twofold axis in the β form. Figures 4a and 4d have the same orientation as far as the molecular geometry is concerned. The difference becomes clear when Figs. 4b and 4c are compared. Nonetheless, the geometry of the CsO_{10} polyhedron in β-$Cs_2V_4O_9$ can still be described as a bicapped square prism. Not surprisingly, the corresponding Cs–O bond lengths are similar and the average Cs–O bond lengths are identical.

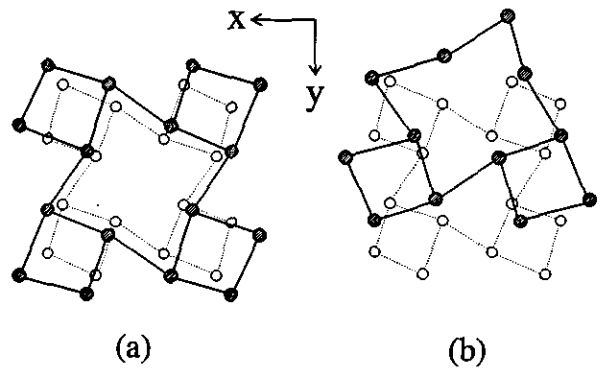

FIG. 5. Stacking of V layers in (a) α-$Cs_2V_4O_9$ and (b) β-$Cs_2V_4O_9$ as viewed down the c-axis.

Powder X-Ray Diffraction of $Cs_2V_4O_9$

Polycrystalline samples of $Cs_2V_4O_9$ as prepared by the solid-state method were well crystallized. TGA data in O_2 indicated that oxidation started rapidly above about 340°C. Weight gain data gave a chemical composition of $Cs_2V_4O_{8.98(1)}$. Thus it is not apparently nonstoichiometric. Its powder X-ray diffraction pattern is similar to that previously reported, but not characterized (5). More reflections, especially in the low-angle region, were observed in this work. Except for a few weak reflections, namely those with d-spacings (Å; relative intensities in brackets) of 4.1505 (I_0 = 3.5%), 3.4397 (2.3%), 2.5537 (6.2%), and 2.2013 (1.6%), the pattern was successfully indexed by the program TREOR90P to a tetragonal cell with a = 5.7302(2) Å, c = 15.0533(8) Å, and high figures of merit $M(25)$ = 63 (29), $F(25)$ = 73 (30). The cell parameters are consistent, within errors, with those of the α-$Cs_2V_4O_9$.

Since the β form was also observed in crystals, efforts were made to index the above unexplained reflections. It was found that when the reflection with d = 4.5576 Å (I_0 = 2.1%), which was indexed for the α phase, was excluded, all other observed lines could be indexed with TREOR90P again to a tetragonal system with essentially the same a-axis but doubled c-axis. This solution is in fact the β phase. When the body-centered symmetry was taken into consideration, a few other peaks (d = 2.5622 Å (I_0 = 7.0%), 2.5260 Å (2.8%), and 2.0140 Å (2.0%)), which could be indexed by both unit cells, could be excluded for the second phase. The final indexing gave a = 5.7305(2) Å and c = 30.1045(14) Å with high figures of merit $M(24)$ = 42 and $F(24)$ = 47 for β-$Cs_2V_4O_9$.

The indexing results suggested the coexistence of the two polytypes in the powder sample. However, indexing alone may not be conclusive because, except for a few weak reflections in each case, there exists significant overlapping between lines from both phases. The Rietveld refinement method with X-ray diffraction data was thus used to confirm this conclusion. The atomic parameters had been well refined in the single-crystal structure analysis. They were held fixed in the profile analysis. Only the scale and profile parameters were allowed to vary. Refinement details are summarized in Table 4. The α-form-only model could fit the whole pattern rather well in general. However, as pointed out above, there were a few weak peaks that could not be explained by α-$Cs_2V_4O_9$, the most prominent of which are marked as I (for body-centered cell) peaks in Fig. 6. The β-form-only model could also fit the whole pattern including the I peaks, but the fit was less satisfactory than the α-form-only model, and the peak (d = 4.5576 Å) marked as P (for primitive cell) could not be accounted for at all. The two-phase refinement was no doubt the best. The final observed, calculated and difference patterns are plotted in Fig. 6 with two rows of tic marks underneath the difference pattern to show Bragg peak positions for the two phases. The fit is seen to be excellent. All observed peaks have been explained, and the final R-factors are better than the individual refinements. Therefore, it is reasonable to conclude that the as-prepared sample of $Cs_2V_4O_9$ is a mixture of the two identified polytypes.

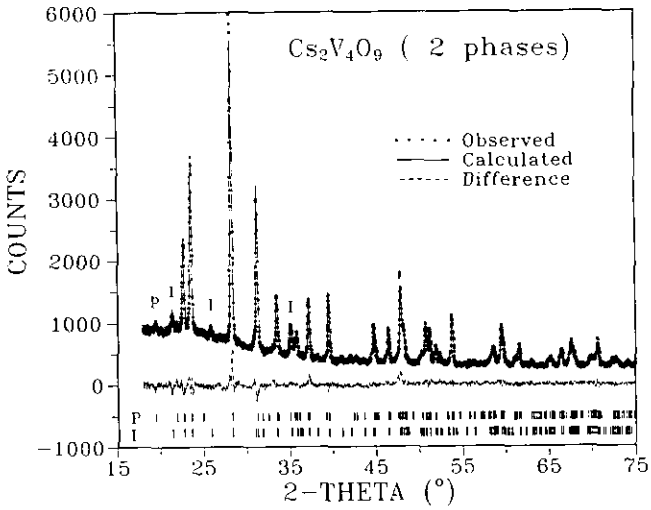

FIG. 6. Observed, calculated, and difference X-ray diffraction patterns of polycrystalline $Cs_2V_4O_9$. See text for details.

Origin of the Two Polytypes of $Cs_2V_4O_9$

The composition of the mixture can be estimated by assuming that the sample contained no other phase(s) except for the two identified. The method used was first proposed and tested by Hill and Howard (31). The equation utilizes the individual Rietveld scale factors (S) from the multiphase profile analysis, the formula weights (M), unit cell volumes (V) and the number of formula units per

TABLE 4
Data Collection Conditions and Rietveld Refinement Details for $Cs_2V_4O_9$ and $Rb_2V_4O_9$[a]

	$Cs_2V_4O_9$				$Rb_2V_4O_9$[b]	
Diffraction method	X-ray				Neutron	X-ray
Wavelength	Cu $K\alpha$				1.3915 Å	Cu $K\alpha$
2θ range (°)	18–75				8–73	10–80
Step size (°)	0.020				0.10	0.030
Profile points (N)	2850				651	2333
Structure model	α-$Cs_2V_4O_9$	β-$Cs_2V_4O_9$	Two phases (α- + β-)		α-$Cs_2V_4O_9$	
Cell parameters						
a (Å)	5.7279(3)	5.7251(4)	5.7270(5)	5.7271(6)	5.665(2)	5.6749(4)
c (Å)	15.051(1)	30.111(2)	15.053(2)	30.103(6)	14.737(6)	14.739(1)
Profile R_P	0.0648	0.0724	0.0487		0.0460	0.0765
Weighted profile R_{WP}	0.0840	0.0986	0.0623		0.0601	0.0990
Expected R_E	0.0412	0.0415	0.0412		0.0342	0.0429
Bragg R_B	0.139	0.182	0.0945	0.112	0.0644	0.128
Goodness of fit	2.04	2.37	1.51		1.76	2.31
Parameters refined (P)	10	10	14		32	26
Preferred orientation vector	(1 1 0)	(1 1 0)	(1 1 0)	(1 1 0)	(0 0 1)	(1 1 0)
Preferred orient. factor, $G1$	0.129(8)	0.258(8)	0.215(31)	0.144(43)	−0.06(2)	0.18(1)
Independent reflections	137	86	137	86	166	155

[a] The R-factors and preferred orientation parameters have been defined in (2).
[b] Two-phase refinement including the $Rb_2V_3O_8$ phase. See text for details.

TABLE 5
Powder X-Ray Diffraction Pattern of α-$Cs_2V_4O_9$

h k l	d_{calc}	d_{obs}	I_{obs}
0 0 2	7.527	7.533	3
1 0 2	4.5593	4.5576	5
1 1 1	3.9126	3.9120	27
0 0 4	3.7633	3.7640	49
1 1 3	3.1524	3.1528	100
2 0 0	2.8651	2.8656	43
2 0 2	2.6777	2.6779	15
1 0 5	2.6652	2.6652	6
2 1 0	2.5626	2.5622	7
2 1 1	2.5263	2.5260	5
0 0 6	2.5089	2.5086	7
1 1 5	2.4166	2.4169	16
2 0 4	2.2796	2.2798	17
2 2 0	2.0259	2.0261	9
1 0 7	2.0134	2.0140	4
2 2 2	1.9563	1.9563	8
1 1 7	1.8995	1.8993	30
2 0 6	1.8875	1.8874	12
3 1 0	1.8120	1.8118	4
3 1 1	1.7991	1.7988	11
3 0 3	1.7851	1.7843	14
3 1 2	1.7617	1.7619	8
3 1 3	1.7043	1.7044	16
2 2 6	1.5762	1.5765	4
3 1 5	1.5525	1.5526	14
0 0 10	1.5053	1.5052	8
4 0 0	1.4325	1.4324	1
4 0 2	1.4073	1.4074	5
3 1 7	1.3857	1.3858	8
3 3 0	1.3506	1.3504	1
3 3 1	1.3452	1.3453	2
4 1 3	1.3394	1.3394	3
2 0 10	1.3326	1.3328	10
3 3 3	1.3042	1.3045	1
2 1 10	1.2980	1.2982	3
3 2 7	1.2781	1.2784	2

Note. Tetragonal, space group $P4_2/m$, a = 5.7302(2) Å, c = 15.0533(8) Å; d-spacings by Guinier method, intensities by diffractometer.

unit cell (Z). Calculations indicated that the $Cs_2V_4O_9$ mixture contained about 55% of the α form and 45% of the β form. That is, both phases are abundant in the mixture. The powder patterns are listed in Tables 5 and 6, respectively. Due to the severe overlap of peaks from both phases, the observed intensities are decomposed and normalized based on the Rietveld refinement results.

To investigate the possibility of a phase transition between the two polytypes in the $Cs_2V_4O_9$ system, two halves of a pellet contained well mixed $2CsVO_3$ and V_2O_3 were simultaneously heated at 510°C for 24 hr then one was air-quenched and the other cooled at 30°C/hr to room temperature. The two products had essentially indistinguishable Guinier X-ray diffraction patterns. The fact that crystals of both phases were obtained during crystal growth from 700°C suggested that no phase transition took place even at 700°C.

Considering the fact that the two phases have very similar structures and essentially the same packing efficiencies, and that they both have high abundances in the mixture, it is quite likely that they formed simultaneously under the experimental conditions (510°C). Even at 400°C, a temperature at which the reaction between $2CsVO_3$ and V_2O_3 became very slow and several intermittent regrindings were necessary to complete the reaction, the product still contained the two phases. Thus the two

TABLE 6
Powder X-Ray Diffraction Pattern of β-$Cs_2V_4O_9$

h k l	d_{calc}	d_{obs}	I_{obs}
0 0 4	7.527	7.533	2
1 0 5	4.1510	4.1505	15
1 1 2	3.9127	3.9120	29
0 0 8	3.7633	3.7640	43
1 0 7	3.4398	3.4397	2
1 1 6	3.1525	3.1528	100
1 0 9	2.8889	2.8907	4
2 0 0	2.8652	2.8656	43
2 0 4	2.6777	2.6779	15
2 1 1	2.5535	2.5537	12
0 0 12	2.5089	2.5086	6
1 1 10	2.4166	2.4169	16
2 1 5	2.3580	2.3583	1
2 0 8	2.2797	2.2798	16
2 1 7	2.2015	2.2013	1
2 2 0	2.0260	2.0261	9
2 2 4	1.9564	1.9563	9
1 1 14	1.8995	1.8993	29
2 0 12	1.8875	1.8874	11
3 1 0	1.8121	1.8118	3
3 1 2	1.7991	1.7988	15
2 2 8	1.7839	1.7843	8
3 1 4	1.7618	1.7619	5
3 1 6	1.7044	1.7044	17
2 2 12	1.5762	1.5765	4
3 2 10	1.5526	1.5526	14
0 0 20	1.5053	1.5052	7
4 0 0	1.4326	1.4324	1
4 0 4	1.4073	1.4074	5
3 1 14	1.3857	1.3858	8
3 3 0	1.3507	1.3504	1
3 3 2	1.3453	1.3453	3
2 0 20	1.3326	1.3328	9
3 3 6	1.3042	1.3045	2

Note. Tetragonal, space group $I\bar{4}2d$, a = 5.7305(2) Å, c = 30.105(1) Å; d-spacings by Guinier method, intensities by diffractometer.

reactions have probably very similar activation energies and the two structures have similar free energies. On the contrary, a transformation between them is expected to have a high activation energy because this would involve major structural changes, the rotation and shifting of the V–O layers, as described above.

Structure of $Rb_2V_4O_9$

Similar to the Cs analogue $Rb_2V_4O_9$ was oxidized in O_2 rapidly above ~340°C. Weight gain data gave a formula slightly higher than its stoichiometric composition, $Rb_2V_4O_{9.05(1)}$. This is believed to be due to the existence of an impurity phase, $Rb_2V_3O_8$, as identified by powder X-ray diffraction. The powder pattern of $Rb_2V_4O_9$ was similar to that previously reported but not characterized (4). It was indexed with TREOR90P to a tetragonal unit cell with a = 5.6774(5) Å and c = 14.744(2) Å with $M(24) = 29$ and $F(24) = 30$, which appears to be isostructural with α-$Cs_2V_4O_9$. The Guinier data are listed in Table 7.

A two-phase refinement was used to refine the structure of $Rb_2V_4O_9$ using both powder neutron and X-ray diffraction data. The procedure has been described previously (32). The structure of $Rb_2V_3O_8$ has been determined recently by single-crystal X-ray diffraction (3, 33); its atomic parameters were not refined. For bond length and bond angle calculations the unit cell parameters and atomic positions for Rb and V from the X-ray data were used, and atomic parameters for O from neutron data were used. Refinement details for $Rb_2V_4O_9$ are listed in Table 4, atomic parameters in Table 8, and selected bond information is listed in Table 3. The neutron and X-ray diffraction patterns are shown in Figs. 7 and 8, respectively. The results have confirmed the α-$Cs_2V_4O_9$ type structure for $Rb_2V_4O_9$. There is no evidence for the existence of a β-$Cs_2V_4O_9$ type $Rb_2V_4O_9$.

The $Rb_2V_4O_9$ structure is less well defined as compared to α-$Cs_2V_4O_9$ due to the limited powder diffraction data. This can be seen from the large estimated standard deviations. The VO_5 square pyramid in $Rb_2V_4O_9$ appears to be more distorted than those in α-$Cs_2V_4O_9$ and β-$Cs_2V_4O_9$. From the two-phase refinement, the impurity level was estimated to be about 12% from neutron data and 15%

TABLE 7
Powder X-Ray Diffraction Pattern of $Rb_2V_4O_9$

h k l	d_{calc}	d_{obs}	I_{obs}
0 0 2	7.3722	7.3538	5
1 0 1	5.2982	5.2917	12
1 1 1	3.8735	3.8706	9
1 0 3	3.7159	3.7136	21
0 0 4	3.6861	3.6850	20
1 1 3	3.1091	3.1088	85
2 0 0	2.8387	2.8379	78
2 0 2	2.6491	2.6486	8
1 0 5	2.6169	2.6173	4
2 1 0	2.5390	2.5389	9
2 1 2	2.4006	2.4002	5
1 1 5	2.3766	2.3755	6
2 0 4	2.2491	2.2496	11
2 2 0	2.0073	2.0067	12
1 0 7	1.9748	1.9749	1
2 2 2	1.9368	1.9365	6
1 1 7	1.8652	1.8651	12
3 1 1	1.7822	1.7821	14
2 1 6	1.7658	1.7648	13
3 1 3	1.6864	1.6859	11
3 1 5	1.5335	1.5343	6
0 0 10	1.4744	1.4744	4
4 2 2	1.2511	1.2508	5

Note. Tetragonal, space group $P4_2/m$, a = 5.6774(5) Å, c = 14.744(2) Å; Guinier data, intensities by film scanner.

TABLE 8
Atomic Parameters of $Rb_2V_4O_9$ from Powder Neutron and X-Ray Data Refinement

Atom	Site	x	y	z	B (Å^2)
		X-ray			
Rb	4j	0.249(2)	0.235(2)	0.5	2.5(2)
V	8k	0.319(2)	0.159(2)	0.2001(3)	2.6(2)
		Neutron			
Rb	4j	0.238(5)	0.224(4)	0.5	6.0(5)
O(1)	2a	0	0	0.25	3.2(7)
O(2)	8k	0.260(3)	0.230(3)	0.0964(7)	3.0(3)
O(3)	8k	0.213(3)	0.393(2)	0.299(1)	4.4(4)

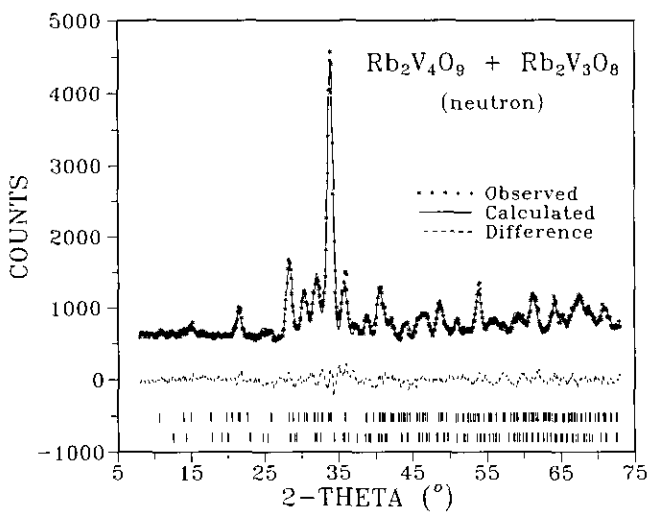

FIG. 7. Observed, calculated, and difference neutron diffraction patterns of $Rb_2V_4O_9$ and the impurity phase $Rb_2V_3O_8$.

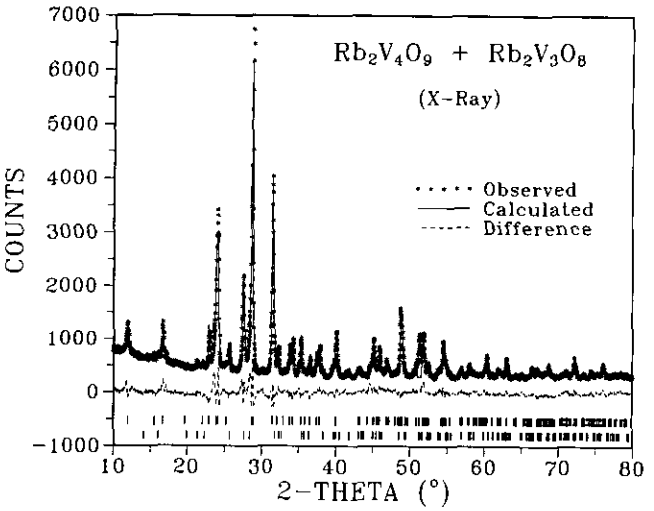

FIG. 8. Observed, calculated, and difference X-ray diffraction patterns of $Rb_2V_4O_9$ and the impurity phase $Rb_2V_3O_8$.

from X-ray data using the same method mentioned above.

Magnetic Properties

Temperature dependencies of the magnetic susceptibility for $Rb_2V_4O_9$ and $Cs_2V_4O_9$ are plotted in Fig. 9. Both samples show a very broad susceptibility maximum at high temperatures, indicating strong short-range magnetic correlations. The low-temperature data suggest that both specimens were contaminated by paramagnetic impurities. As stated above, the $Rb_2V_4O_9$ sample contained about 12–15% $Rb_2V_3O_8$, which is known to become antiferromagnetic below 10 K (3). The impurity level in $Cs_2V_4O_9$ appears to be much lower than in $Rb_2V_4O_9$.

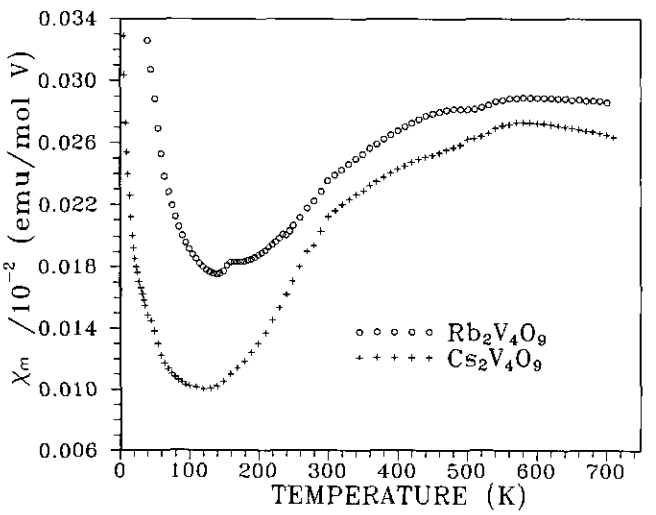

FIG. 9. Thermal variations of the magnetic susceptibility of polycrystalline $Rb_2V_4O_9$ and $Cs_2V_4O_9$.

As will be shown below, the magnetic behavior is predominantly influenced by the individual V–O layers. The α- and β-$Cs_2V_4O_9$ structures are very much alike in this sense. Thus short-range magnetic correlations are not believed to be significantly different for the two polytypes.

The layered structures of the above vanadium oxides suggest that the magnetic short-range order is likely two-dimensional (2D) or lower, namely, one-dimensional (1D, or infinite linear chain). Due to the lack of sufficient data above the susceptibility maxima a detailed quantitative fit to the appropriate models is not likely to be reliable.

It is well known nonetheless that the exchange coupling constant, $|J|$, and the powder-averaged g-factor are related to the maximum susceptibility temperature, T_{max}, and the maximum susceptibility, χ_{max}, by some constants for a given type of short-range order. The arrangement of the magnetic vanadium atoms in these oxides can be approximated as square planar (Fig. 5). The relationships are

$$\frac{kT_{max}}{|J|} = 1.871 \qquad [1]$$

$$\frac{\chi_{max}|J|}{Ng^2\mu_B^2} = 0.0469 \qquad [2]$$

for an $S = \frac{1}{2}$ 2D Heisenberg square planar system (34), and

$$\frac{kT_{max}}{|J|} = 1.282 \qquad [3]$$

$$\frac{\chi_{max}|J|}{Ng^2\mu_B^2} = 0.07346 \qquad [4]$$

for the $S = \frac{1}{2}$ 1D Heisenberg model (35), where S is the spin quantum number and μ_B the Bohr magneton. $|J|$ can be estimated from [1] and [3], and g from [2] and [4]. For the above two systems, the paramagnetic impurity contributions are very small at high temperatures and are neglected in the calculations. The obtained parameters are summarized in Table 9.

The estimated g-factors are quite small for the 1D model as compared with those for other VO_5 coordination oxides with V(IV), for example, $g \approx 1.9$ for $A_2V_3O_8$ (A = K, Rb, NH_4) (3) and $g \approx 1.8$ for CaV_3O_7 and SrV_3O_7 (2). Those for the 2D model are slightly higher, but seem to be more reasonable considering the fact that a correction for temperature-independent paramagnetism was not included, which would reduce the maximum susceptibilities and, thus, the g factors. Therefore, the parameters appear to favor the 2D model for $A_2V_4O_9$ (A = Rb, Cs), in

TABLE 9
Magnetic Parameters for $Rb_2V_4O_9$ and $Cs_2V_4O_9$

Compound	T_{max} (K)	χ_{max} (emu/mole)	2D model		1D model	
			$\|J\|/k$(K)	g	$\|J\|/k$(K)	g
$Rb_2V_4O_9$	590	2.89×10^{-4}	315	2.27	460	1.61
$Cs_2V_4O_9$	590	2.73×10^{-4}	315	2.21	460	1.56

contrast to the best fit to the 1D model for the AV_3O_7 system (2).

The coupling constants $|J|$ for $Rb_2V_4O_9$ and $Cs_2V_4O_9$ are significantly higher than those for the AV_3O_7 series (A = Cd, Ca, Sr) (2). As shown earlier, the two systems have similar layer structures. Cs^+ and Rb^+ are much larger in size than the A^{2+} ions (18) and thus have stronger basicity than the latter ions. Therefore, the observed magnetic behavior is clearly in support of the inductive mechanism previously proposed for the AV_3O_7 system.

The sharp susceptibility anomaly at about 160 K for $Rb_2V_4O_9$ is likely an indication of the onset of long-range magnetic order. The origin of additional anomalies at about 500 K for both samples is not clear. DSC data for both samples showed no thermal anomalies up to 670 K. Thus, these high-temperature anomalies are not believed to be due to phase transitions. The infection at about 50 K for $Cs_2V_4O_9$ is near the known transition temperature for solid O_2, a common contaminant in the SQUID magnetometer.

No spin-flop transition, which is normally a signature of long-range order, could be observed for $Rb_2V_4O_9$ at low temperatures (Fig. 10). On the other hand, it is likely that the two polytypes of $Cs_2V_4O_9$ have two different long-range orders due to the different stacking sequences of the V–O layers. A preliminary neutron scattering experiment at 10 K showed no new peaks due to magnetic scattering for $Cs_2V_4O_9$.

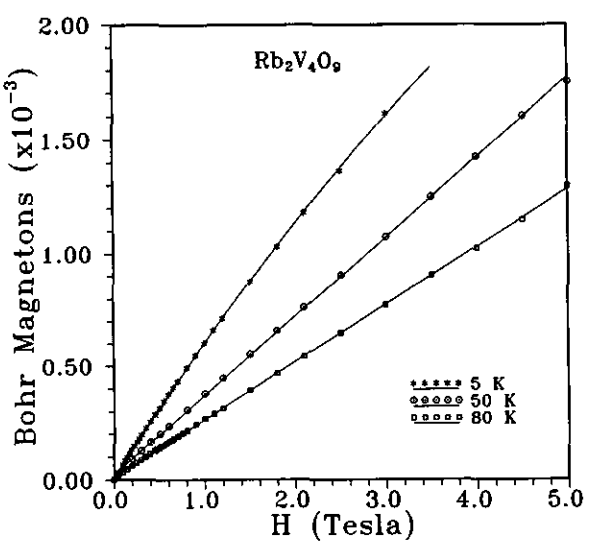

FIG. 10. Magnetization curves of $Rb_2V_4O_9$ at various temperatures.

ACKNOWLEDGMENTS

We thank Dr. Jim Britten for collecting the single-crystal X-ray diffraction data and for his many helpful discussions, and Mr. Frank Gibbs for performing the thermal analysis. Special thanks to Dr. Susan M. Kauzlarich and Ms. Stephanie Brock at the University of California at Davis for obtaining the high-temperature magnetic data. The financial support of the Natural Science and Engineering Research Council of Canada and the Ontario Centre for Materials Research is acknowledged gratefully.

REFERENCES

1. J.-C. Bouloux and J. Galy, *Acta Crystallogr. Sect. B* **29,** 269 (1973).
2. Guo Liu and J. E. Greedan, *J. Solid State Chem.* **103,** 139 (1993).
3. Guo Liu and J. E. Greedan, *J. Solid State Chem.*, in press.
4. J. Tudo and B. Jolibois, *C. R. Acad. Sci. Ser. C* **273,** 1526 (1971).
5. A. A. Fotiev and L. L. Surat, *Russ. J. Inorg. Chem. (Engl. Transl.)* **24,** 735 (1979).
6. Guo Liu and J. E. Greedan, *J. Solid State Chem.* **103,** 228 (1993)
7. J. E. Greedan, Guo Liu, B. W. Arbuckle, K. V. Ramanujachary, and M. Greenblatt, *J. Solid State Chem.* **97,** 419 (1992).
8. P. E. Werner, L. Eriksson, and M. Westdahl, *J. Appl. Crystallogr.* **18,** 367 (1985).
9. D. B. Wiles and R. A. Young, *J. Appl. Crystallogr.* **14,** 149 (1981).
10. C. S. Pratt, B. A. Coyle, and J. A. Ibers, *J. Chem. Soc. A*, 2146 (1971).
11. P. W. Selwood, "Magnetochemistry," 2nd ed., p. 78. Interscience, New York, 1956.
12. M. Catti and G. Ferraris, *Acta Crystallogr. Sect. A* **32,** 163 (1976).
13. H. D. Flack, *Acta Crystallogr. Sect. A* **39,** 876 (1983).
14. G. Bernardinelli and H. D. Flack, *Acta Crystallogr. Sect. A* **41,** 500 (1985).
15. I. D. Brown and D. Altermatt, *Acta Crystallogr. Sect. B.* **41,** 244 (1985).
16. J.-C. Bouloux and J. Galy, *Acta Crystallogr. Sect. B* **29,** 1335 (1973).
17. J.-C. Bouloux and J. Galy, *J. Solid State Chem.* **16,** 385 (1976).
18. R. D. Shannon, *Acta Crystallogr. Sect. A* **32,** 751 (1976).
19. M. Dion, Y. Piffard, and M. Tournoux, *J. Inorg. Nucl. Chem.* **40,** 917 (1978).
20. A. Verbaere and M. Tournoix, *Bull. Soc. Chim. Fr.* **3,** 1237 (1973).
21. See, for example, J. Galy, *J. Solid State Chem.* **100,** 229 (1992).
22. W. G. Mumme and J. A. Watts, *J. Solid State Chem.* **3,** 319 (1971);

K. Waltersson and B. Forslund, *Acta Crystallogr. Sect. B* **33,** 789 (1977).
23. K. Waltersson and B. Forslund, *Acta Crystallogr. Sect. B* **33,** 784 (1977).
24. M.-L. Ha-Eierdanz and U. Müller, *Z. Anorg. Allg. Chem.* **613,** 63 (1992).
25. Yu. E. Gorbunova, S. A. Linde, A. V. Lavrov, and I. V. Tananaev, *Dokl. Akad. Nauk. SSSR* **250,** 350 (1980); K. H. Lii and S. L. Wang, *J. Solid State Chem.* **82,** 239 (1989).
26. K. H. Lii and W. C. Liu, *J. Solid State Chem.* **103,** 38 (1993).
27. K. Waltersson and B. Forslund, *Acta Crystallogr. Sect. B* **33,** 780 (1977).
28. K. Waltersson and B. Forslund, *Acta Crystallogr. Sect. B* **33,** 775 (1977).
29. P. M. de Wolff, *J. Appl. Crystallogr.* **1,** 108 (1968).
30. G. S. Smith and R. L. Snyder, *J. Appl. Crystallogr.* **12,** 60 (1979).
31. R. J. Hill and C. J. Howard, *J. Appl. Crystallogr.* **20,** 467 (1987).
32. Guo Liu and J. E. Greedan, *J. Solid State Chem.* **110,** 274 (1994).
33. M.-L. Ha-Eierdanz and Ulrich Müller, *Z. Anorg. Allg. Chem.* **613,** 63 (1992).
34. R. Navarro, *in* "Magnetic Properties of Layered Transition Metal Compounds" (L. J. de Jongh, Ed.). Kluwer, Dordrecht, 1990.
35. W. E. Hatfield, *J. Appl. Phys.* **52,** 1985 (1981).